Accuracy of pencil-beam redefinition algorithm dose calculations in patient-like cylindrical phantoms for bolus electron conformal therapy

Robert L. Carver[a] and Kenneth R. Hogstrom
Mary Bird Perkins Cancer Center, 4950 Essen Lane, Baton Rouge, Louisiana 70809 and Department of Physics and Astronomy, Louisiana State University, Baton Rouge, Louisiana 70803

Connel Chu and Robert S. Fields
Mary Bird Perkins Cancer Center, 4950 Essen Lane, Baton Rouge, Louisiana 70809

Conrad P. Sprunger
Department of Physics and Astronomy, Louisiana State University, Baton Rouge, Louisiana 70803

(Received 5 March 2013; revised 28 May 2013; accepted for publication 28 May 2013; published 18 June 2013)

Purpose: The purpose of this study was to document the improved accuracy of the pencil beam redefinition algorithm (PBRA) compared to the pencil beam algorithm (PBA) for bolus electron conformal therapy using cylindrical patient phantoms based on patient computed tomography (CT) scans of retromolar trigone and nose cancer.
Methods: PBRA and PBA electron dose calculations were compared with measured dose in retromolar trigone and nose phantoms both with and without bolus. For the bolus treatment plans, a radiation oncologist outlined a planning target volume (PTV) on the central axis slice of the CT scan for each phantom. A bolus was designed using the planning.decimal® (p.d) software (.decimal, Inc., Sanford, FL) to conform the 90% dose line to the distal surface of the PTV. Dose measurements were taken with thermoluminescent dosimeters placed into predrilled holes. The Pinnacle^3 (Philips Healthcare, Andover, MD) treatment planning system was used to calculate PBA dose distributions. The PBRA dose distributions were calculated with an in-house C++ program. In order to accurately account for the phantom materials a table correlating CT number to relative electron stopping and scattering powers was compiled and used for both PBA and PBRA dose calculations. Accuracy was determined by comparing differences in measured and calculated dose, as well as distance to agreement for each measurement point.
Results: The measured doses had an average precision of 0.9%. For the retromolar trigone phantom, the PBRA dose calculations had an average $\pm 1\sigma$ dose difference (calculated − measured) of −0.65% ± 1.62% without the bolus and −0.20% ± 1.54% with the bolus. The PBA dose calculation had an average dose difference of 0.19% ± 3.27% without the bolus and −0.05% ± 3.14% with the bolus. For the nose phantom, the PBRA dose calculations had an average dose difference of 0.50% ± 3.06% without bolus and −0.18% ± 1.22% with the bolus. The PBA dose calculations had an average dose difference of 0.65% ± 6.21% without bolus and 1.75% ± 5.94% with the bolus. From a clinical perspective an agreement of 5% or better between planned (calculated) and delivered (measured) dose is desired. Statistically, this was true for 99% ($\pm 2\sigma$) of the dose points for three of the four cases for the PBRA dose calculations, the exception being the nose without bolus for which this was true for 89% ($\pm 1.6\sigma$) of the dose points. For the retromolar trigone, with and without bolus, the PBA showed agreement of 5% or better for approximately 86% ($\pm 1.5\sigma$) of the dose points. For the nose, with and without bolus, the PBA showed agreement of 5% or better for only approximately 58% ($\pm 0.8\sigma$) of the dose points.
Conclusions: The measured data, whose high precision makes them useful for evaluation of the accuracy of electron dose algorithms, will be made publicly available. Based on the spread in dose differences, the PBRA has at least twice the accuracy of the PBA. From a clinical perspective the PBRA accuracy is acceptable in the retromolar trigone and nose for electron therapy with and without bolus. [http://dx.doi.org/10.1118/1.4811104]

Key words: electron conformal therapy, electron bolus, pencil beam redefinition algorithm, electron dose calculation

I. INTRODUCTION

Electron beam therapy (EBT) with beams of approximately 4–20 MeV is an established modality for treating disease lying within 6 cm of the patient's surface, particularly for sites of the chest wall, head, and neck.[1,2] Electron beams produce dose distributions characterized by a reasonably uniform dose (e.g., 90%–100%) from the surface or near the surface to the depth of the distal 90% dose line (R_{90}) and a sharp dose falloff from 90% to 10% ($R_{90\text{-}10}$). This quality allows a

single electron beam to be used for a planning target volume (PTV) while sparing distal normal tissue. Typically, the lowest beam energy that provides an R_{90} greater than the deepest PTV depth is utilized; however, if the distal PTV depth beneath the surface varies, then needless dose is delivered to normal tissue distal to the PTV. This needless dose can be reduced by multiple electron conformal therapy (ECT) technologies, reviewed by Hogstrom *et al.*[3] All ECT methods aim to conform the 90% dose surface to the distal surface of the PTV. One of these methods, bolus ECT, which uses a variable thickness wax bolus placed on the patient surface to conform the distal 90% dose surface to the PTV, is commercially available (BolusECT®, .decimal, Inc., Sanford, FL). Bolus ECT has been shown useful for multiple sites in the head and neck, postmastectomy chest wall, and paraspinal muscles.[4–10]

Increased dose conformity to the PTV requires an accurate dose calculation algorithm for bolus design and treatment planning. Currently, many clinics use a form of the pencil beam algorithm (PBA), developed by Hogstrom *et al.*[11] and implemented by Starkschall *et al.*,[12] for electron dose calculations in their treatment planning system (TPS). This algorithm has known deficiencies in the presence of certain types of patient heterogeneities, particularly bone, and air cavities.[11,13–17] Other pencil beam algorithms, such as the generalized Gaussian model,[18] show similar deficiencies.[19] The presence of such heterogeneities in the head and neck region, where ECT is commonly used, means that a more accurate electron dose algorithm could be beneficial.

The pencil beam redefinition algorithm (PBRA) developed by Shiu and Hogstrom[20] and refined by Boyd *et al.*[21] has been shown to be highly accurate for heterogeneities in a water phantom[22] and in four patient sites (nose, postmastectomy chest wall, internal mammary chain, and paraspinal muscles).[23] This algorithm was implemented recently into commercial software for the design of electron bolus (planning.decimal® or p.d from .decimal, Inc., Sanford, FL). The PBRA is well suited for utilization with bolus design in that it requires the same beam commissioning data as the PBA, making it as easy to commission as the PBA, and its computation time should be substantially faster than fast Monte Carlo (MC) methods,[24,25] which benefits multiple dose calculations utilized in the bolus design process.[26]

With the recent commercial availability of bolus ECT, knowing the accuracy of the PBA and PBRA dose calculations in the presence of bolus is of clinical interest. A recent study of the accuracy of the dose delivery of bolus ECT and mixed beam therapy (intensity-modulated x-ray therapy optimized on top of bolus ECT dose distributions) to chest wall and parotid PTVs embedded in a homogeneous cylindrical phantom by Kavanaugh *et al.*[27] showed for the bolus ECT dose component that the PBA calculations agreed with measured data to within 4% or 2 mm for 98.8% and 97.3% of points for parotid and chest wall plans, respectively. Kavanaugh[28] showed similar accuracy for the PBRA, i.e., dose calculations agreed with measured data to within 4% or 2 mm for 98.9% and 98.7% of points for the same parotid and chest wall plans, respectively. However, PBA and PBRA accuracies are not expected to be similar in the presence of patient internal heterogeneities.

The purpose of this study was to document the improved accuracy of the PBRA as compared to the PBA for cylindrical patient phantoms of the retromolar trigone and nose that were based on patient CT scans, particularly in the presence of bolus. These phantoms were the identical ones used previously to document the accuracy of the PBA upon its original commercial release in a treatment planning system[13] (RTPlan, General Electric, Medical Systems Division, Milwaukee, WI). High precision dose measurements consisting of multiple thermoluminescent dosimeter (TLD) measurements were made for one treatment plan without bolus and one with conformal bolus for each of the two phantoms.

II. METHODS

II.A. Phantom description

Electron dose distributions were measured for two cylindrical patient-like phantoms with and without bolus. The two cylindrical phantoms used in this study were the same ones used to estimate PBA accuracy in patients previously treated for a retromolar trigone and nose cancer.[13] The axial cross section of each phantom was based on the mid-PTV CT scan of a patient. The phantoms, constructed of SR4 muscle substitute, SR4 bone substitute, and air cavities, allowed insertion of TLD capsules for dose measurement (cf. Fig. 1).

II.B. Treatment planning

For the nonbolus cases, CT scan data were imported into the Pinnacle[3] (Philips, Andover, MD) treatment planning system (TPS). The CT scans were taken at 120 kVp, a pitch of 0.562, and a beam width of 20 mm with a GE LightSpeed 16 slice scanner. The cylindrical phantoms were scanned such that the transverse CT slices were perpendicular to their cylindrical axis. Reconstructed transverse CT slices were spaced every 2.5 mm, and in the image plane 512 × 512 pixels covered an area 25 × 25 cm^2. For purposes of both PBA and PBRA dose calculation, all CT images were modified by filling the phantom holes with the CT number for water.

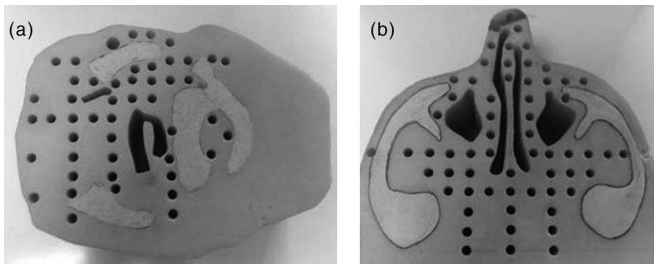

FIG. 1. Cylindrical phantoms (height perpendicular to axial plane = 7 cm) from Hogstrom *et al.* (Ref. 13) were composed of bone and muscle tissue substitutes to model CT scans of patients with (a) retromolar trigone and (b) nose cancer. These 2D phantoms have a constant axial cross section with the exception of the holes drilled to house plastic TLD capsules or water.

The treatment planning parameters such as field size, source-to-surface distance (SSD), and beam energy were taken from Hogstrom *et al.*[13] For the retromolar trigone phantom, a field size of 7.2 × 8.6 cm^2 (10 × 10 cm^2 applicator) at 100 cm SSD was used with the 8.6 cm width in the plane of measurement. The 16 MeV beam ($E_{p,o}$ = 16.6 MeV) on the Clinac EX (Varian Medical Systems, Palo Alto, CA) was used in the present study, as compared to the 17 MeV beam ($E_{p,o}$ = 16.3 MeV) used by Hogstrom *et al.* For the nose phantom, a field size of 8 × 8 cm^2 (10 × 10 cm^2 applicator) at 96 cm SSD was used. The 12 MeV beam ($E_{p,o}$ = 12.6 MeV) was used, as compared to the 13 MeV beam ($E_{p,o}$ = 12.1) used by Hogstrom *et al.* In both cases the SSD was the central-axis distance from a point 100 cm above isocenter to the phantom surface.

For the bolus cases, a radiation oncologist outlined a PTV on the central axis slice of the CT scan that simulated treatment of parotid and nose cancer for the retromolar trigone and nose phantoms, respectively. These PTVs were extended along the cylindrical axis, creating cylindrically symmetric PTVs covering the entire height of the phantoms. The PTVs drawn by the radiation oncologist were typical of what is seen in the clinic and not the same as the PTVs of the original study, which were unavailable. Hence, the field size and energies of the bolus ECT plans were not the same as those in Hogstrom *et al.*[13] The initial field sizes were created with a 1-cm margin. Treatment plans with these PTVs were then exported to the p.d software, which was used to design boluses via forward planning that conformed the 90% dose surface to the distal surface of the PTV. The p.d software used the standard operators described in Low *et al.*[26] for bolus design and the PBRA for dose calculation. For the retromolar trigone phantom, the bolus was designed using the p.d operator sequence: Creation, Smooth, Truncate, Isodose Shift, Smooth; Truncate reduces the thickness of the unmilled part of the bolus and has no impact on the calculated dose. For the nose phantom, the p.d operator sequence was Flat Top, Surface Shift, and Truncate, i.e., a bolus surface, flat and perpendicular to the beam central axis, was created then shifted to 3 mm below the tip of the nose (cf. Fig. 9). Next, the field widths in the plane of measurement were manually adjusted using the p.d dose calculations so as to improve conforming of the 90% dose surface to the part of the distal PTV surface lying near the field edge. Using that field width the bolus design was redone using the same operator sequence. The resulting bolus shapes were imported back into the TPS for PBA dose calculation.

Following approval of the dose distributions in the TPS, the bolus designs were sent electronically by the p.d software to .decimal for fabrication. After each of the bolus arrived at our site each phantom was rescanned with its respective bolus in place. These CT scans, taken using the same protocol as the original CT scans, were imported into the TPS for a final dose calculation using the PBA. This quality assurance check, identical to that used with patients,[4] verified that the fabricated bolus met the design criteria and that the resulting dose distributions adequately conformed to the PTVs. Both PBA and PBRA dose calculations for these CT data sets were used for comparison with measured data.

For the final dose calculations and irradiations, the retromolar trigone phantom was planned using the 16 MeV beam at 105 cm SSD with a 7.8 × 11.8 cm^2 (defined at isocenter) cerrobend insert in the 15 × 15 cm^2 applicator, where the 11.8 cm defined the field width in the plane of measurement. The nose phantom was planned using the 16 MeV beam at 100 cm SSD with a 8.0 × 9.8 cm^2 (defined at isocenter) cerrobend insert in the 10 × 10 cm^2 applicator, where the 9.8 cm defined the field width in the plane of measurement. In both cases the SSD was the central axis distance from a point 100 cm above isocenter to the bolus surface; the 105 cm SSD was required to allow clearance between the bolus and applicator.

II.C. Dose calculations

The accuracy of PBA and PBRA dose calculations was evaluated by comparing with the measured dose points for the phantoms using the treatment plans described above. The PBA dose distribution was obtained from the Pinnacle^3 TPS. The beam energies used in this experiment had been commissioned for clinical use in the TPS using the standard techniques described in Hogstrom and Steadham.[14]

As p.d does not export the PBRA dose calculations used for bolus design, doses were calculated by the research version of the PBRA, upon which the p.d software was based. The PBRA was commissioned using the same measured data set used to commission the PBA for the TPS. The PBRA uses the same central-axis percent depth doses and some of the same commissioning parameters as the PBA (e.g., $\sigma_{\theta x}$ and L_0). Table I lists the beam parameters used for the PBA and PBRA calculations.

A CT lookup table was configured to correspond to the specific materials that composed the phantoms. The table's values were determined using separate sample pieces of SR4 muscle and bone, and a CT scan of these pieces. Calculated values for the linear stopping and scattering powers for the pieces were determined using the NIST ESTAR database (http://physics.nist.gov/PhysRefData/Star/Text/ESTAR.html) and ICRU 35,[29] respectively, for the chemical composition of the SR4 bone and muscle[30] and their measured densities. The NIST and ICRU 35 data were combined with the measured CT values to create the CT number to linear stopping power and scattering powers table (relative to water) shown in Table II. For the bolus ECT dose calculations the wax bolus was also included in the CT lookup table with the stopping and scattering powers determined by Low and Hogstrom.[31]

TABLE I. PBA and PBRA beam parameters for the Varian Clinac EX 12 and 16 MeV beams used for this study.

Nominal energy (MeV)	$E_{p,o}$ (PBA only) (MeV)	$\sigma_{\theta x}$ (mrad)	L_0 (cm)	FMCS (PBA only)
12	12.56	32.5	7.0	1.2
16	16.62	29.0	7.0	1.2

TABLE II. Correlation of CT number to relative stopping and scattering powers for tissue substitute phantom materials. The two rows with CT numbers of 870 and 915 were used only for phantoms with bolus.

CT number	Relative stopping power	Relative scattering power	Material
0	0.001	0.001	Air
870	0.912	0.717	Wax bolus
915	0.959	0.754	
920	0.959	0.827	SR4 muscle
990	1.032	0.890	
1000	1.000	1.000	Water
1050	1.094	0.944	SR4 muscle
1150	1.199	1.034	
1950	1.524	2.162	SR4 bone
2500	1.953	2.771	

PBA and PBRA dose calculations were made using the CT value of each voxel to determine the relative stopping and scattering power used by the dose calculations, just as is done in patients. Figure 2 compares plots of the relative linear stopping and scattering powers versus CT number with a histogram of the CT numbers for the retromolar trigone phantom with bolus scan.

II.D. Dose measurements

The phantom exposures were made on a Varian Clinac 21EX using electron beam energies of 12 and 16 MeV. The doses were measured using approximately 45 mg samples of LiF TLD-100 powder (Rexon Components, Inc., Beachwood, OH) contained in cylindrical polyethylene TLD containers

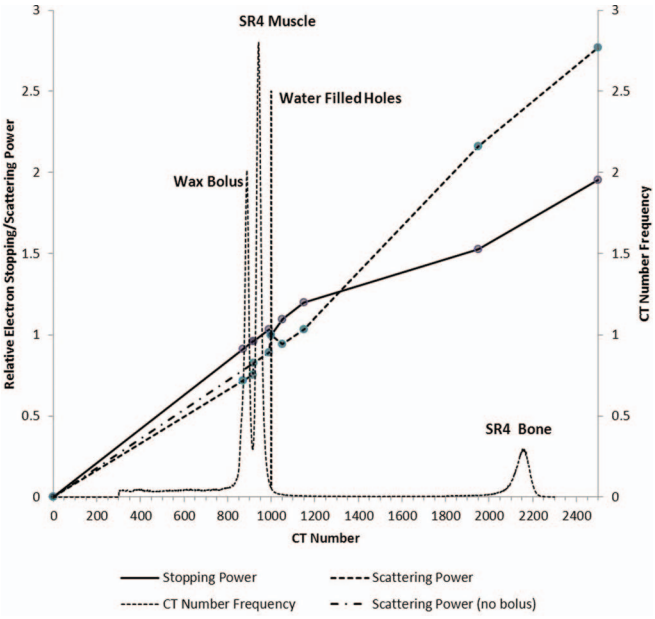

FIG. 2. Plot showing the relative linear stopping and scattering powers versus CT number from Table II. Superimposed is the distribution of CT numbers for the retromolar trigone phantom with bolus. The solid circles represent the data points contained in the CT lookup table.

that could be inserted into predrilled holes in each phantom. There were 47 and 62 locations in the retromolar trigone and nose phantoms, respectively. The TLD containers were constructed of polyethylene tubing with an outer diameter of 5 mm and an inner diameter of 3 mm so that the 3 mm diameter polyethylene plugs fit snugly into the containers.

The lengths of the containers were 5 and 6 cm, respectively, so that they protruded and were easily inserted and removed from the phantoms. The TLD powder occupied a volume 3 mm in diameter by 5 mm long. The TLD powder was sandwiched between polyethylene plugs such that upon full insertion into the phantom the center of the TLD powder volume was at the midplane of the phantom.

For irradiation, the phantoms were laid flat on a 5 cm thick slab of water-equivalent plastic resting on the treatment couch with the drilled holes vertical. The gantry was rotated 90° to irradiate using a horizontal beam. After alignment to the beam, the outline of the phantom and the alignment laser projections were traced onto the plastic slab so that phantom-beam alignment could be verified prior to each TLD exposure. The phantoms were irradiated multiple times, with each irradiation exposing a single row of TLDs perpendicular to the beam direction starting with the row closest to the machine head. As the TLD measurement row moved downstream the upstream holes were filled with water, as modeled in the PBA and PBRA calculations. TLD holes downstream of the measurement row were always empty.

First, measurements were taken for the phantoms without the use of bolus. For each phantom, monitor units were determined to deliver a given dose of 200 cGy. Given dose is defined as the central axis dose maximum in a water phantom set to the treatment plan's SSD and irradiated using the plan's collimation. The retromolar trigone and nose phantoms were exposed with the 16 and 12 MeV beams, respectively, in accordance with the treatment plans. Each phantom was exposed on two different days (1 TLD per hole per day). For readout, the TLD powder was divided into three approximately 12.5 mg samples to obtain three dose readings for each TLD, resulting in a total of six dose readings for each measurement position.

Independent of the first set of measurements, a second set of measurements was taken for each phantom using variable thickness bolus ECT. For each phantom, monitor units were determined to deliver a given dose of 222.2 cGy (200 cGy to the 90% dose line). The retromolar trigone and nose phantoms were exposed with the 16 MeV beams in accordance with the treatment plans. Each phantom was exposed twice on the same day. At readout, again the TLD powder was divided into three approximately 12.5 mg samples to obtain three dose values for each TLD, resulting in a total of six dose values for each measurement position.

Each sample of powder was analyzed using a UL-320 TLD reader (Rexon Components, Inc., Beachwood, OH). Prior to readout the approximately 12.5 mg samples were weighed using an AL54 scale (Mettler-Toledo, LLC, Columbus, OH). Samples were spread evenly on a planchette and analyzed at least 2 days after irradiation. The TL signal per unit mass TL/m (counts/mg) was recorded.

II.E. TLD readout and analysis

For the nonbolus exposures, calibration TLDs were exposed at R_{100} in a water-equivalent plastic phantom for the 10 × 10 cm^2 open applicator and energy of interest to absolute doses of 20, 50, 100, 200, and 240 cGy. During each day of TLD readout a set of calibration TLDs, exposed on the same day as were the phantom TLDs, was analyzed to determine that day's calibration curve. The calibration curve was determined by fitting a quadratic function to a plot of average readout, $\overline{(TL/m)}_{net}$, versus dose, where $(TL/m)_{net} = (TL/m)_{gross} - (TL/m)_{bkgd}$. All further references of TL/m readings refer to $(TL/m)_{net}$.

A slightly different calibration technique was used for readout of the bolus ECT TLDs exposed. A single calibration curve was measured using doses of 0, 50, 100, 150, 200, 220, 275, and 325 cGy. Again a quadratic function was fit to the plot of $\overline{TL}/m$ versus dose. On each day of phantom TLD readout, results of calibration TLDs exposed to a dose of 220 cGy on the same day as the phantom TLDs were used to scale the single calibration curve. All calibration curves exhibited a slight supralinearity, but were within 5% of being linear over the selected dose range.

For the nonbolus phantoms a sample mass correction was made to the TL/m values due to an observed correlation with sample mass. The change in TL/m caused by varying the mass (m) of samples exposed to a dose of 200 cGy was measured. Normalized to a mass of 12.5 mg, a corrected value, $(TL/m)_{corr}$, was fit with a linear curve given by $(TL/m)_{corr} = (TL/m) \times (0.0159m + 0.801)$. This correction was applied to obtain the $(TL/m)_{corr}$ values, which were converted to dose using the calibration curve described above. Due to observations of this mass effect during readout of the nonbolus TLDs ($\sigma = 1.4$ mg), care was taken so that the sample masses used during the bolus TLD readouts were more uniform ($\sigma = 0.5$ mg), which allowed the sample mass correction to be ignored for the bolus TLD readouts.

For dose comparisons, both the calculated and measured doses were normalized such that 100% equaled the given dose, i.e., the comparison was of absolute, not relative doses. For the nonbolus dose distributions the data were normalized so that the given dose of 200 cGy was 100%. For the bolus dose distributions the data were normalized so that the given dose of 222.2 cGy was 100% (200 cGy was 90%). For comparison, measured dose points inside circles were superimposed onto isodose plots. Also, the percent dose difference (calculated − measured) and the distance-to-agreement (DTA) were determined for each dose measurement point for purposes of comparison.

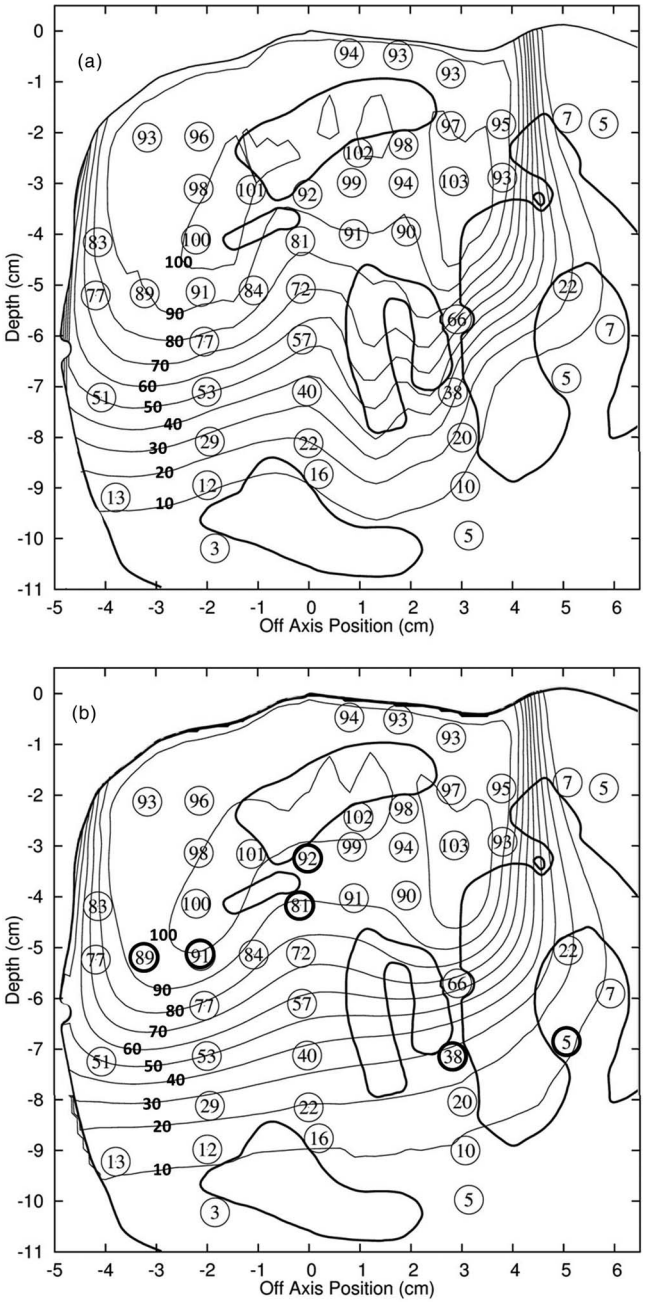

FIG. 3. Measured TLD doses ($N = 47$) for the retromolar trigone phantom without bolus (16 MeV) superimposed on isodose plots of the (a) PBRA and (b) PBA calculated dose distributions. Isodose values are labeled in bold. The locations of the phantom's mandibles, spinal column, pharynx, and skin surface are outlined. Points having a dose difference >5% and a DTA > 3 mm are indicated by bold circles.

III. RESULTS

III.A. Retromolar trigone dose plan without bolus

Figure 3 shows the measured dose points superimposed on the PBRA and PBA dose calculations for the retromolar phantom treatment plan without bolus. Figure 4 shows histograms of the dose differences as well as whether points have a DTA greater or less than 3 mm for the PBRA and PBA. For the PBRA there was an average dose difference of −0.65% with a standard deviation of 1.86%; for the PBA there was an average dose difference of 0.19% with a standard deviation of 3.39%. These standard deviations are significant compared to 0.9%, the average standard error for the mean TLD measured dose values, and root-mean-square (rms) subtraction of this error resulted in PBRA and PBA standard errors for dose differences of 1.62% and 3.27%, respectively.

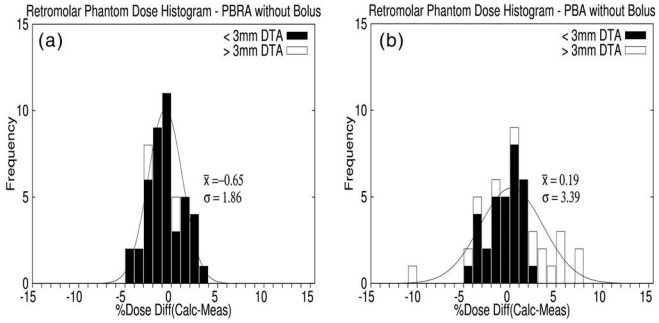

FIG. 4. Dose difference histograms ($N = 47$) for the retromolar trigone phantom without bolus for the (a) PBRA and (b) PBA. The parameters of the superimposed Gaussian curve are the average and standard deviation of the measured dose differences. Points with a DTA less (greater) than 3 mm are histogrammed in black (white).

For the PBA, the point with a dose difference in the $(-11\%, -10\%)$ interval is the measured 38% dose point located anterior to the vertebral body and adjacent to the posterior left edge of the pharynx. There are two points in the (7%, 8%) interval; one is the measured 81% dose point located medial to the anterior medial edge of the right mandible, and one is the measured 91% dose point located medial and anterior to the right mandible. There are three points in the (5%, 6%) interval; one is the measured 92% dose point located adjacent to the anterior medial edge of the right mandible; one is the 89% dose point located medial and anterior to the right mandible; and one is the measured 5% dose point located interior to the vertebral body. These points are indicated by bold circles in Fig. 3(b). The rest of the dose points are within 5% of the measured values. For the PBRA, all calculation points lie within 5% of the measured values.

III.B. Nose dose plan without bolus

Figure 5 shows the measured dose points superimposed on the PBRA and PBA dose calculations for the nose treatment plan without bolus. Figure 6 shows histograms of the dose differences as well as whether points have a DTA greater or less than 3 mm for the PBRA and PBA. For the PBRA, there was an average dose difference of 0.5% with a standard deviation of 3.19%; for the PBA there was an average dose difference of 0.65% with a standard deviation of 6.27%. Again, rms subtraction of the average experimental error resulted in PBRA and PBA standard errors for dose differences of 3.06% and 6.21%, respectively.

The PBRA dose distribution shows six points with a dose difference of greater than 5% [cf. Fig. 5(a)], but it is important to note that all of these points have a DTA less than 3 mm with all but one occurring in high-dose-gradient regions caused by scatter in the nose. The PBA shows points with a dose difference greater than 5% with 19 having a DTA greater than 3 mm. The PBA calculation contains seven points with a dose difference greater than 10% and DTA greater than 3 mm located largely in the septum region and posterior to the sinus cavities [cf. Fig. 5(b)]. These differences are consistent with the PBA's limitations in handling heterogeneities that are

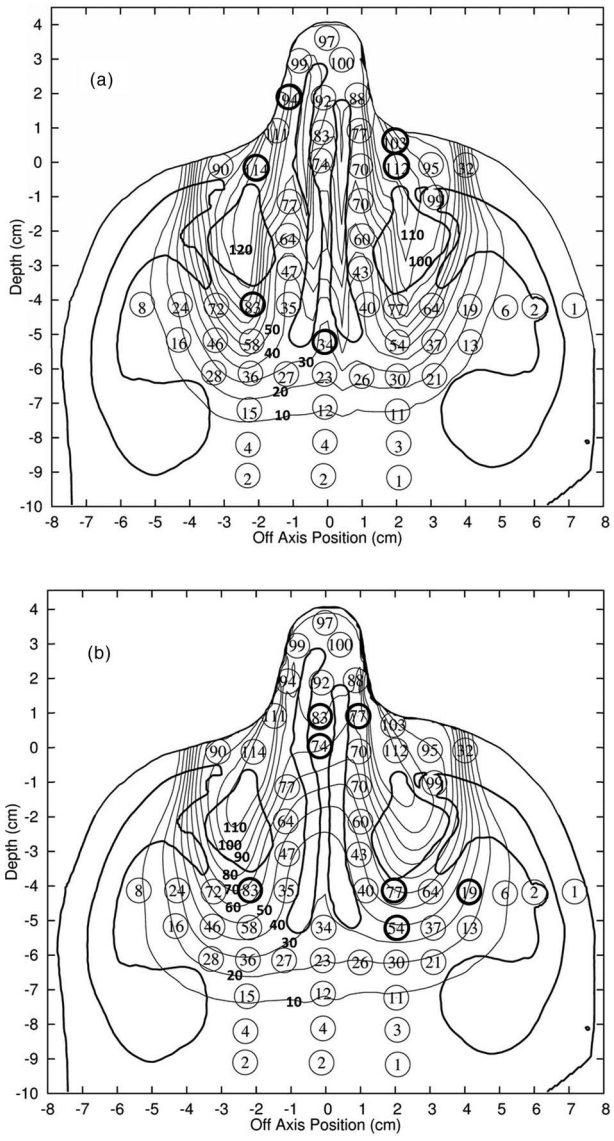

FIG. 5. Measured TLD doses ($N = 59$) for the nose phantom without bolus (12 MeV) superimposed on isodose plots of the (a) PBRA and (b) PBA calculated dose distributions. Isodose lines are labeled in bold. The locations of the phantom's mandibles, nasal and sinus cavities, and skin surface are outlined. Points having a dose difference >5% and a DTA < 3 mm in (a) and a dose difference >10% and a DTA > 3 mm in (b) are indicated by bold circles.

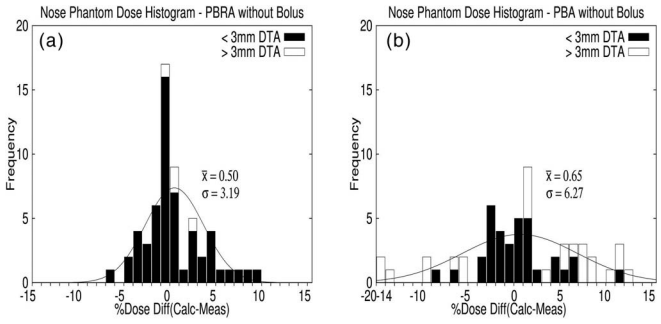

FIG. 6. Dose difference histograms ($N = 59$) for the nose phantom without bolus for the (a) PBRA and (b) PBA. The parameters of the superimposed Gaussian curve are the average and standard deviation of the measured dose differences. Points with a DTA less (greater) than 3 mm are histogrammed in black (white).

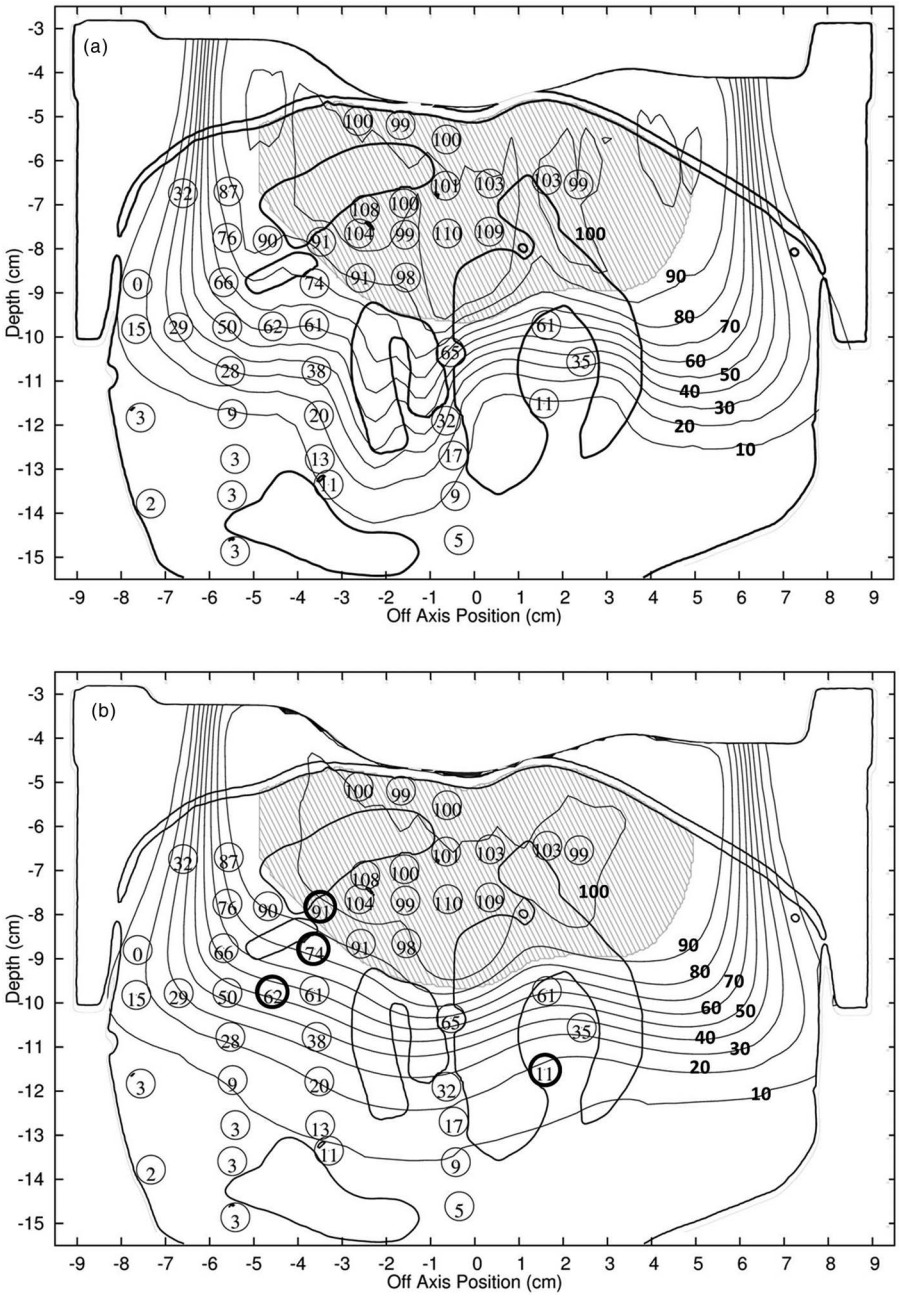

FIG. 7. Measured TLD doses ($N = 46$) for the retromolar trigone phantom with bolus (16 MeV) superimposed on isodose plots of the (a) PBRA and (b) PBA calculated dose distributions. Isodose lines are labeled in bold. The shaded region represents the physician delineated PTV; the narrow band between the phantom and bolus is a small air gap. Points having a dose difference >5% and a DTA > 3 mm are indicated by bold circles.

either vertical and narrow (septum) or deep (sinus cavities and maxillary antrum bone).

III.C. Retromolar dose plan with bolus

Figure 7 shows the measured dose points superimposed on the PBRA and PBA dose calculations for the retromolar trigone treatment plan with bolus. Figure 8 shows histograms of the dose differences as well as whether points have a DTA greater or less than 3 mm for the PBRA and PBA. For the PBRA, there was an average dose difference of −0.20% and a standard deviation of 1.78%; for the PBA, there was an average dose difference of −0.05% and a standard deviation of 3.27%. Again, rms subtraction of the average experimental error resulted in PBRA and PBA standard errors for dose difference of 1.54% and 3.14%, respectively.

The PBA dose distribution has four points with a dose difference of greater than 5% and a DTA greater than 3 mm [cf. Fig. 7(b)]; three of these points are the measured 91%, 74%, and 62% points medial to the anterior edge of the right mandible, and the fourth point is the measured 11% point located inside the spinal column. The PBRA dose distibution has no points with a dose difference greater than 5% and DTA greater than 3 mm.

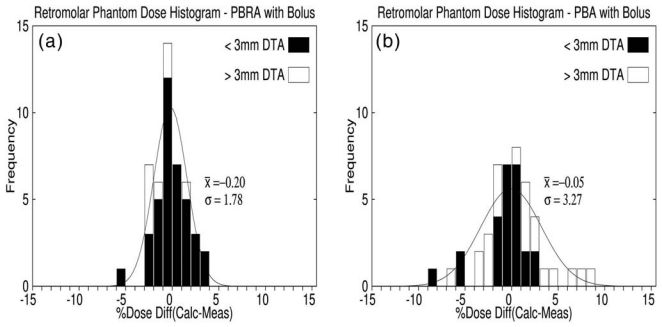

FIG. 8. Dose difference histograms ($N = 46$) for the retromolar trigone phantom with bolus for the (a) PBRA and (b) PBA. The parameters of the superimposed Gaussian curve are the average and standard deviation of the measured dose differences. Points with a DTA less (greater) than 3 mm are histogrammed in black (white).

III.D. Nose dose plan with bolus

Figure 9 shows the measured dose points superimposed on the PBRA and PBA dose calculations for the nose treatment plan with bolus. Figure 10 shows histograms of the dose differences as well as whether points have a DTA greater or less than 3 mm for the PBRA and PBA. For the PBRA, there was an average dose difference of −0.18% and a standard deviation of 1.52%; for the PBA, there was an average dose difference of 1.75% and a standard deviation of 6.01%. Again, rms subtraction of the average experimental error resulted in PBRA and PBA standard errors for the dose difference of 1.22% and 5.94%, respectively.

The PBA distribution shows 27 points with a dose difference of greater than 5%, all with a DTA greater than 3 mm. The seven points with the largest differences (>8%) were located on the row of measurement points immediately distal to the sinus cavities [cf. Fig. 9(b)]. These differences are expected in the PBA due to the bolus resulting in the sinus and mandible heterogeneities being deeper. The PBA agreement in the septum region was improved relative to the nonbolus plan by the bolus creating a more uniform distribution in the PTV. The PBRA distribution shows all points within 5% of the measured value and only one point outside of 4%.

IV. DISCUSSION

IV.A. PBA accuracy

For the plans without bolus, a comparison of the accuracy previously reported by Hogstrom *et al.*[13] and the current PBA accuracy, using the criteria described in Hogstrom *et al.*, showed the two dose calculations to be qualitatively similar. Hogstrom *et al.* separated points into low dose gradient regions (LGR) and high dose gradient regions (HGR), where the LGR points were evaluated based on dose difference and the HGR points were evaluated based on DTA. For the retromolar phantom PBA calculations, present results showed 87% of the points within 5% or 3 mm, compared to Hogstrom *et al.* who showed 72% within 5% or 3 mm. For the nose phantom PBA calculations, present results showed 58% of the points within 5% or 3 mm, compared to Hogstrom *et al.* who showed 67% within 5% or 3 mm. Such similar results were expected since the beam energies, field sizes, and SSD used in both studies were close to identical. Also, the 2D PBA implementation used by Hogstrom *et al.* and the current 3D PBA implementation are equivalent for the 2D cylindrical phantoms used in this study and should give identical results. Although the scanned beam used in the previous study had a sharper dose fall off ($R_{90\text{-}10}$) in depth than that of the beams used in the current study, this would not be expected to have any significant effect.

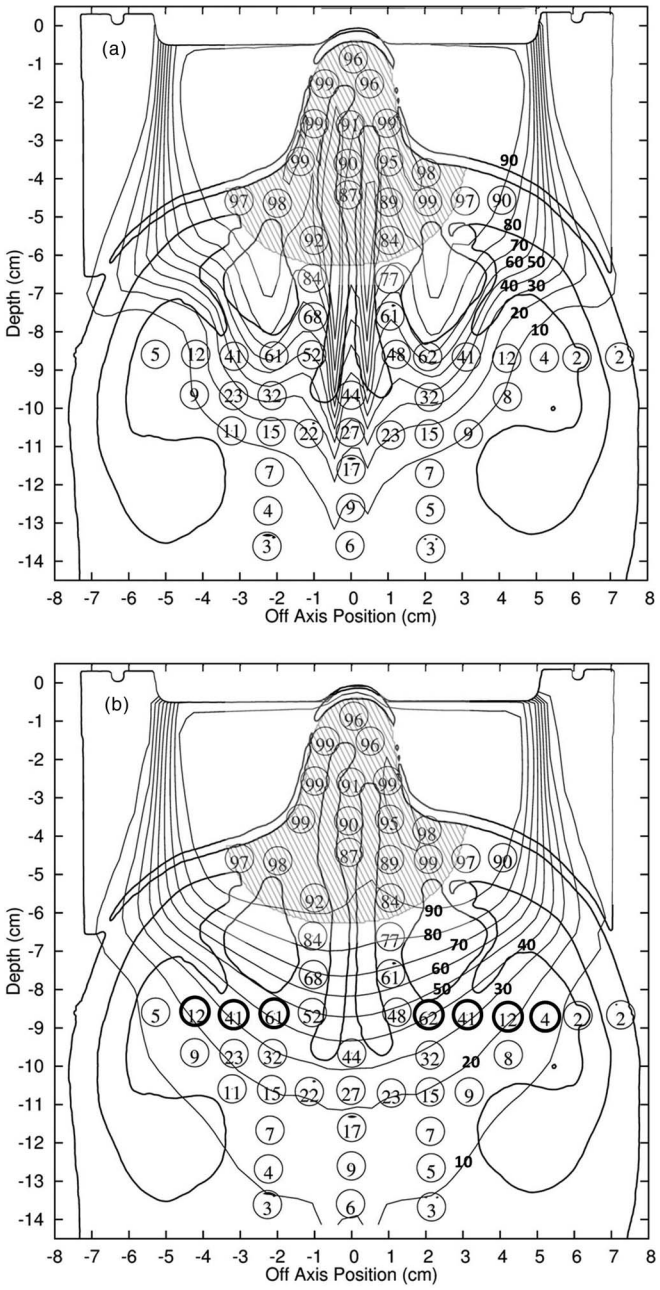

FIG. 9. Measured TLD doses ($N = 57$) for the nose phantom with bolus superimposed with the calculated dose distributions for (a) PBRA and (b) PBA. Isodose lines are labeled in bold. The shaded region represents the physician delineated PTV; the narrow band between the phantom and the bolus is a small air gap. Points having a dose difference >8% and a DTA > 3 mm are indicated by bold circles.

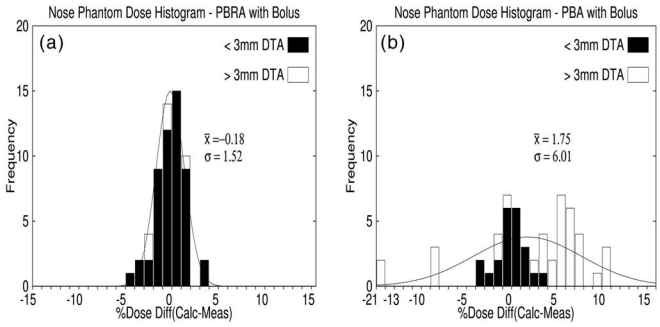

FIG. 10. Dose difference histograms ($N = 57$) for the nose phantom with bolus for the (a) PBRA and (b) PBA. The parameters of the superimposed Gaussian curve are the average and standard deviation of the measured dose differences. Points with a DTA less (greater) than 3 mm are histogrammed in black (white).

For the retromolar trigone phantom, the addition of bolus had little effect on the overall accuracy of the dose plan. The PBA had an average dose difference (±1 standard deviation) of 0.19% ± 3.27% without the bolus compared to −0.05% ± 3.14% with bolus. This result was expected because the addition of this bolus did not greatly deepen the heterogeneities. The PBA bolus plan has four points with a dose difference greater than 5% and DTA greater than 3 mm compared to six points for the plan without bolus. This slight increase in accuracy was not surprising due to the increased dose homogeneity in the PTV region when bolus is used.

For the PBA nose plans, the addition of bolus resulted in the PBA having an average dose difference (±1 standard deviation) of 0.65% ± 6.21% without bolus compared to 1.75% ± 5.94% with bolus. The deepening of the heterogeneities, due to the overlying bolus, caused the PBA to underestimate further the effects of the sinus cavities. This underestimation resulted in an underprediction of the dose distal to these cavities and thus increased the average dose difference. For both cases, the standard deviation was comparably large and possibly unacceptable by today's standards; however it would not be standard practice to treat the nose without placing bolus inside the nasal cavities.[32] Such bolus should decrease the volume of air in the nasal cavities and hence improve the accuracy of the dose calculation.

IV.B. PBRA accuracy

The PBRA dose plans proved to be more accurate than the PBA plans for each phantom-bolus combination measured. For the retromolar trigone phantom, the use of bolus had little effect on the accuracy of the PBRA dose plan. The PBRA plan had an average dose difference ±1 standard deviation of −0.65% ± 1.62% without bolus compared to −0.20 ± 1.54% with bolus. Both dose plans showed all points within 5% or 3 mm of the measured values.

For the nose phantom, the addition of bolus increased the accuracy of the PBRA dose calculations. The PBRA had an average dose difference (±1 standard deviation) of 0.5% ± 3.06% without bolus and −0.18% ± 1.22% with bolus. The increased accuracy is attributed to the use of bolus, which increased the homogeneity of the dose distribution in the anterior nose and septum regions, reducing the magnitude of the high-dose-gradient regions there.

Our results are comparable in accuracy to previous studies by Boyd,[23] who compared PBRA with MC patient dose calculations in four different anatomical sites (parotid, ethmoid sinus, postmastectomy chest wall, and paraspinal muscles). Boyd demonstrated for a parotid plan that the PBRA dose plan agreed with MC to within 4% or 2 mm DTA for 97% of the points in the transverse plane and for 99% of the points in the coronal plane, whereas our results for the retromolar trigone phantom showed 100% of the points within 4% or 3 mm. Boyd also showed for an ethmoid sinus plan that the PBRA dose plan agreed to within 4% or 2 mm DTA for 97% of the points in the transverse plane and 95% of the points in the sagittal plane, whereas our results for the nose phantom (without bolus) showed 100% of the points within 4% or 3 mm.

IV.C. Summary of results

The results from all comparisons are summarized in Table III. The absolute doses of both the PBA and PBRA calculations were accurate, i.e., the average dose difference agreed to within 0.7% for seven of the eight cases, with the exception being the PBA bolus calculation in the nose which was 1.75%. For the PBRA dose calculations, the standard deviation of the dose differences, a good measure of the accuracy of the calculation, was less than 2% for three of the four dose plans with the exception being the nose plan without bolus, which was 3.06%. For the PBA, the standard deviation of the dose difference was approximately a factor of two greater for three of the four cases, being almost four times greater for the nose with bolus plan.

From a clinical perspective an agreement of 5% or better between planned (calculated) and delivered (measured) dose is desired. Statistically, this was true for 99% ($\pm 2\sigma$) of the dose points for three of the four cases for the PBRA dose calculations [cf. Figs. 4(a), 8(a), and 10(a)], the exception being the nose without bolus for which this was true for 89% ($\pm 1.6\sigma$) of the dose points [cf. Fig. 6(a)].

For the retromolar trigone, with and without bolus, the PBA showed agreement of 5% or better for approximately 86% ($\pm 1.5\sigma$) of the dose points [cf. Figs. 4(b) and 8(b)]. For the nose, with and without bolus, the PBA showed agreement of 5% or better for only approximately 58% ($\pm 0.8\sigma$) of the dose points [cf. Figs. 6(b) and 10(b)].

TABLE III. Accuracy of PBRA versus PBA for the retromolar trigone and nose phantoms with and without bolus.

		No bolus (%)	Bolus (%)
Retromolar trigone	PBRA	0.65 ± 1.62	−0.20 ± 1.54
	PBA	0.19 ± 3.27	−0.05 ± 3.14
Nose	PBRA	0.50 ± 3.06	−0.18 ± 1.22
	PBA	0.65 ± 6.21	1.75 ± 5.94

IV.D. Availability of data set

The data set generated for the current study is for head phantoms based on patient anatomy and has a high degree of precision, making it useful for evaluating the accuracy of electron beam dose algorithms. Although data for heterogeneous phantoms has been publicly available previously,[33,34] data in the presence of electron bolus has not. It is the intention of the authors to make the present data set available to the scientific community for the purpose of comparing the accuracy of electron dose algorithms, particularly for the use of bolus ECT.

V. CONCLUSION AND RECOMMENDATIONS

The quality of the TLD data set makes it useful for the evaluation and intercomparison of the accuracy of electron dose algorithms in the head and neck for electron beam treatments without and with bolus. The accuracy of electron dose algorithms, measured as the spread in the distribution of the difference in calculated and measured doses, showed that of the PBRA to be 0.50 and 0.49 that of the PBA without bolus for the retromolar trigone and nose phantoms, respectively, and 0.49 and 0.21 that of the PBA with bolus for the retromolar trigone and nose phantoms, respectively.

From a clinical perspective, the accuracy of the PBA is acceptable (<5%) for the retromolar trigone phantom both with and without bolus. Although the accuracy of the PBA exceeds the 5% criteria for the nose phantom without bolus, its significance should not be overinterpreted, as the error would significantly decrease if bolus is used to fill the nose cavities and to eliminate the surface irregularities of the nose.

The accuracy of the PBRA is clinically acceptable for the retromolar trigone and nose phantoms with and without bolus. Utilization of the PBRA for bolus ECT design is not only desirable, but should calculate dose that agrees well with dose algorithms that have superseded the PBA in treatment planning systems, e.g., macro MC in Eclipse (Varian Medical Systems, Palo Alto, CA)[35] and voxel based Monte Carlo (VMC) in Xio (Elekta AB, Stockholm, Sweden).[36] Also, in bolus ECT when attempting to conform the high dose region to a PTV, a dose algorithm with the accuracy of the PBRA is recommended.

ACKNOWLEDGMENT

This work was supported in part by a research agreement between Mary Bird Perkins Cancer Center and .decimal, Inc.

[a]Electronic mail: rcarver@marybird.com

[1]N. D. Tapley, *Clinical Applications of the Electron Beam* (Wiley, New York, 1976).
[2]J. M. Vaeth and J. L. Meyer, *The Role of High Energy Electrons in the Treatment for Cancer* (S. Karger, New York, 1991).
[3]K. R. Hogstrom, J. A. Antolak, R. J. Kudchadker, C. M. Ma, and D. D. Leavitt, "Modulated electron therapy," in *Proceedings of the 2003 AAPM Summer School, Intensity Modulated Radiation Therapy—The State of the Art*, edited by J. Palta and R. Mackie (Medical Physics, Madison, 2003), pp. 749–786.
[4]D. A. Low, G. Starkschall, N. E. Sherman, S. W. Bujnowski, J. R. Ewton, and K. R. Hogstrom, "Computer-aided design and fabrication of an electron bolus for treatment of the paraspinal muscles," Int. J. Radiat. Oncol., Biol., Phys. **33**, 1127–1138 (1995).
[5]B. Zackrisson and M. Karlsson, "Matching of electron beams for conformal therapy of target volumes at moderate depths," Radiother. Oncol. **39**, 261–270 (1996).
[6]G. H. Perkins, M. D. McNeese, J. A. Antolak, T. A. Buchholz, A. E. Strom, and K. R. Hogstrom, "A custom three dimensional electron bolus technique for optimization of postmastectomy irradiation," Int. J. Radiat. Oncol., Biol., Phys. **51**, 1142–1151 (2001).
[7]R. J. Kudchadker, K. R. Hogstrom, A. S. Garden, M. D. McNeese, R. A. Boyd, and J. A. Antolak, "Electron conformal radiotherapy using bolus and intensity modulation," Int. J. Radiat. Oncol., Biol., Phys. **53**, 1023–1037 (2002).
[8]R. J. Kudchadker, J. A. Antolak, W. H. Morrison, P. F. Wong, and K. R. Hogstrom, "Utilization of custom electron bolus in head and neck radiotherapy," J. Appl. Clin. Med. Phys. **4**, 321–333 (2003).
[9]O. A. Zeidan, B. D. Chauhan, W. W. Estabrook, T. R. Willoughby, R. R. Manon, and S. L. Meeks, "Image-guided bolus electron conformal therapy—A case study," J. Appl. Clin. Med. Phys. **12**, 68–75 (2010).
[10]M. M. Kim, R. J. Kudchadker, J. E. Kanke, S. Zhang, and G. H. Perkins, "Bolus electron conformal therapy for the treatment of recurrent inflammatory breast cancer: A case report," Med. Dosim. **37**, 208–213 (2012).
[11]K. R. Hogstrom, M. D. Mills, and P. R. Almond, "Electron beam dose calculations," Phys. Med. Biol. **26**, 445–459 (1981).
[12]G. Starkschall, A. S. Shiu, S. W. Bujnowski, L. L. Wang, D. A. Low, and K. R. Hogstrom, "Effect of dimensionality of heterogeneity corrections on the implementation of a three-dimensional electron pencil-beam algorithm," Phys. Med. Biol. **36**, 207–227 (1991).
[13]K. R. Hogstrom, M. D. Mills, J. A. Meyer, J. R. Palta, D. E. Mellenberg, R. T. Meoz, and R. S. Fields, "Dosimetric evaluations of a pencil-beam algorithm for electrons employing a two-dimensional heterogeneity correction," Int. J. Radiat. Oncol., Biol., Phys. **10**, 561–569 (1984).
[14]K. R. Hogstrom and R. S. Steadham, "Electron beam dose computation," in *Proceedings of the 1996 Summer School of the AAPM, Teletherapy: Present and Future*, edited by J. Palta and T. R. Mackie (Advanced Medical, Madison, 1996), pp. 137–174.
[15]K. R. Hogstrom and P. Almond, "Review of electron beam therapy physics," Phys. Med. Biol. **51**, R455–R490 (2006).
[16]J. Cygler, J. J. Battista, J. W. Scrimger, E. Mah, and J. A. Antolak, "Electron dose distributions in experimental phantoms: A comparison with 2D pencil beam calculations," Phys. Med. Biol. **32**, 1073–1086 (1987).
[17]E. Mah, J. A. Antolak, J. W. Scrimger, and J. J. Battista, "Experimental evaluation of a 2D and 3D electron pencil beam algorithm," Phys. Med. Biol. **34**, 1179–1194 (1989).
[18]I. Lax and A. Brahme, "Electron beam dose planning using Gaussian beams," Acta Radiol. **24**, 75–85 (1985).
[19]G. X. Ding, J. E. Cygler, C. W. Yu, N. I. Kalach, and G. Daskalov, "A comparison of electron beam dose calculation accuracy between treatment planning systems using either a pencil beam or a Monte Carlo algorithm," Int. J. Radiat. Oncol., Biol., Phys. **63**, 622–633 (2005).
[20]A. S. Shiu and K. R. Hogstrom, "Pencil-beam redefinition algorithm for electron dose distributions," Med. Phys. **18**, 7–18 (1991).
[21]R. A. Boyd, K. R. Hogstrom, and I. I. Rosen, "Effects of using an initial polyenergetic spectrum with the pencil beam redefinition algorithm for electron dose calculations in water," Med. Phys. **25**, 2176–2185 (1998).
[22]R. A. Boyd, K. R. Hogstrom, and G. Starkshall, "Electron pencil-beam redefinition algorithm dose calculations in the presence of heterogeneities," Med. Phys. **28**, 2096–2104 (2001).
[23]R. A. Boyd, "Pencil beam redefinition algorithm dose calculations for electron therapy treatment planning," Ph.D. thesis, University of Texas Health Science Center, Houston, TX, 2001.
[24]H. Neuenschwander and E. J. Born, "A macro Monte Carlo method for electron beam dose calculations," Phys. Med. Biol. **37**, 107–125 (1992).
[25]I. Kawrakow, M. Fippel, and K. Friedrich, "3D electron dose calculation using a Voxel based Monte Carlo algorithm (VMC)," Med. Phys. **23**,445–457 (1996).

[26]D. A. Low, G. Starkschall, S. W. Bujnowski, L. L. Wang, and K. R. Hogstrom, "Electron bolus design for radiotherapy treatment planning: Bolus design algorithms," Med. Phys. **19**, 115–124 (1992).
[27]J. A. Kavanaugh, K. R. Hogstrom, C. Chu, R. L. Carver, J. P. Fontenot, and G. Henkelmann, "Delivery confirmation of bolus electron conformal therapy combined with intensity modulated X-ray therapy," Med. Phys. **40**, 021724 (14pp.) (2013).
[28]J. A. Kavanaugh, "Evaluation of the pencil beam algorithm and pencil beam redefinition algorithm for bolus electron conformal therapy dose computation," M.S. thesis, Louisiana State University, Baton Rouge, LA, 2011, see http://etd.lsu.edu/docs/available/etd-07062011-175440/.
[29]International Commission on Radiation Units and Measurements, "Radiation dosimetry: Electron beams with energies between 1 and 50 MeV," ICRU Report No. 35 (ICRU Publications, Bethesda, MD, 1984).
[30]U. Schneider, E. Pedroni, and A. Lomax, "The calibration of CT Hounsfield units for radiotherapy treatment planning," Phys. Med. Biol. **41**, 111–124 (1996).
[31]D. A. Low and K. R. Hogstrom "Determination of the relative linear collision stopping power and linear scattering power of electron bolus material," Phys. Med. Biol. **39**, 1063–1068 (1994).
[32]K. R. Hogstrom, "Electron beam therapy: Dosimetry, planning and techniques," in *Principles and Practice of Radiation Oncology*, edited by C. Perez, L. Brady, E. Halperin, and R. Schmidt-Ullrich (Lippincott Williams and Wilkins, Baltimore, 2003), pp. 252–282.
[33]R. A. Boyd, K. R. Hogstrom, J. A. Antolak, and A. S. Shiu, "A measured data set for evaluating electron-beam dose algorithms," Med. Phys. **28**, 950–958 (2001).
[34]A. S. Shiu, S. Tung, K. R. Hogstrom, J. W. Wong, R. L. Gerber, W. B. Harms, J. A. Purdy, R. K. Ten Haken, D. L. McShan, and B. A. Fraass, "Verification data for electron beam dose algorithms," Med. Phys. **19**, 623–636 (1992).
[35]R. A. Popple, R. Weinber, J. A. Antolak, S. J. Ye, P. N. Pareek, J. Duan, S. Shen, and I. A. Brezovich, "Comprehensive evaluation of a commercial macro Monte Carlo electron dose calculation implementation using a standard verification data set," Med. Phys. **33**, 1540–51 (2006).
[36]P. Edimo, M. G. Kwato Njock, and S. Vynckier, "Validation of XiO electron Monte Carlo-based calculations by measurements in a homogeneous phantom and by EGSnrc calculations in a heterogeneous phantom," Phys. Med. (in press) (2012). [Available online 23 September 2012].